SLAC-PUB-7198
June, 1996

A PRELIMINARY MEASUREMENT OF THE b QUARK FRAGMENTATION FUNCTION IN HADRONIC Z^0 DECAYS*

The SLD Collaboration**

Stanford Linear Accelerator Center

Stanford University, Stanford, CA 94309

* This work was supported by Department of Energy contracts: DE-FG02-91ER40676 (BU), DE-FG03-92ER40701 (CIT), DE-FG03-91ER40618 (UCSB), DE-FG03-92ER40689 (UCSC), DE-FG03-93ER40788 (CSU), DE-FG02-91ER40672 (Colorado), DE-FG02-91ER40677 (Illinois), DE-AC03-76SF00098 (LBL), DE-FG02-92ER40715 (Massachusetts), DE-AC02-76ER03069 (MIT), DE-FG06-85ER40224 (Oregon), DE-AC03-76SF00515 (SLAC), DE-FG05-91ER40627 (Tennessee), DE-AC02-76ER00881 (Wisconsin), DE-FG02-92ER40704 (Yale); National Science Foundation grants: PHY-91-13428 (UCSC), PHY-89-21320 (Columbia), PHY-92-04239 (Cincinnati), PHY-88-17930 (Rutgers), PHY-88-19316 (Vanderbilt), PHY-92-03212 (Washington); the UK Science and Engineering Research Council (Brunel and RAL); the Istituto Nazionale di Fisica Nucleare of Italy (Bologna, Ferrara, Frascati, Pisa, Padova, Perugia); and the Japan-US Cooperative Research Project on High Energy Physics (Nagoya, Tohoku).

Ref: PA04-044
Submitted to the 28th International conference on High Energy Physics, Warsaw, Poland, July 25-31,1996

ABSTRACT

We present a measurement of the *b* quark fragmentation function from a sample of semi-leptonic B decays collected between 1993 and 1995 in the SLD experiment at SLAC. The energy of each tagged B hadron was reconstructed using information from the lepton and a partially-reconstructed charm-decay vertex. A comparison of the scaled energy distribution with several phenomenological models of heavy quark fragmentation was made, using the same model in each case to correct the data. The average scaled energy was found to be $\langle x_E \rangle = 0.697 \pm 0.012(stat)^{+0.028}_{-0.024}(syst)$ (preliminary).

1 Introduction

By virtue of the large *b* mass, one expects that in $e^+e^- \to b\bar{b}$ events the *b* quark* will fragment into a B hadron which carries, on average, a large fraction x_E of the beam energy. In $Z^0 \to b\bar{b}$ decays the *b* quark fragmentation function has been measured by studying the lepton momentum spectrum [1] in semileptonic B decays, and has focused on extracting the mean scaled B energy fraction $\langle x_E \rangle$. Such a procedure does not allow for a precise measurement of the shape of the fragmentation function. Recently measurements of the distribution of x_E have been reported [2, 3, 4], yielding values consistent with $\langle x_E \rangle \approx 0.70$. These measurements, performed using semileptonic-B samples [2, 3] or an inclusive B sample [4], are sensitive to the procedure used to unfold the data [5] for the effects of bin-to-bin migration due to misassigned energy in the B energy reconstruction.

The shape of the *b* quark fragmentation function $D_b(x_E, Q^2)$ at a c.m. energy *Q* can be calculated in perturbative QCD [6,7] and can also be predicted by phenomenological models such as the Peterson [S], Lund [9] and Bowler [10] models. It is important to check the validity of the QCD and model predictions. In addition, a measurement of $D_b(x, Q^2)$ at $Q = m_{Z^0}c^2$, when compared with lower- (or higher-) energy measurements, allows for a measurement of QCD scaling violations in the fragmental ion function. Finally, a number of B physics studies [11] depend upon a knowledge of the shape of the *b* quark fragmentation function, so that better experimental constraints will serve to reduce systematic errors in these measurements. The procedure described here to measure the primary B energy in each event may be useful to analyses [12] where the proper time $t = l/\gamma v$, where $\gamma = E_B/m_B$, l is the decay length, m_B is the B hadron mass, and v is the velocity of the B hadron, must be known quite well.

In this analysis we use the SLD precision tracking system to select $Z^0 \to b\bar{b}$ decays, where B hadrons are identified via $B \to DlX$ decays. The charmed hadron D is identified

* Unless stated otherwise, charge-conjugate states are also implied.

from a secondary decay vertex formed from charged tracks, and the lepton l ($l = e$ or μ) is required to have large momentum transverse to the B flight direction. Energy depositions, measured in the hermetic calorimeter, that are not associated to the Dl system are subtracted from the jet energy to yield the reconstructed B hadron energy. The energy distribution is then unfolded for analysis and selection biases to yield the b fragmentation function.

2 Apparatus and Hadronic Event Selection

The e^+e^- annihilation events produced at the Z^0 resonance by the SLAC Linear Collider (SLC) have been recorded using the SLC Large Detector (SLD). A general description of the SLD can be found elsewhere [13]. This analysis used charged tracks measured in the central drift chamber (CDC) [14] and the vertex detector (VXD) [15], energy clusters measured in the Liquid Argon Calorimeter (LAC) [16], and muon tracks measured in the Warm Iron Calorimeter (WIC) [17]. Momentum measurement is provided by a uniform axial magnetic field of 0.6 T. The CDC and VXD give a momentum resolution of $\sigma^2[(\text{ GeV/c})^{-2}] = (0.0026)^2 + (0.0095/p)^2$, where p is the track momentum in GeV/c. Including the uncertainty on the primary interaction point (IP), they give a combined impact parameter resolution of $11 \oplus 76/(p_\perp \sqrt{\sin\theta})$ μm, where $p_\perp$ is the track momentum transverse to the beam axis in GeV/c and θ is the polar angle with respect to the beamline. The result is a typical 2-prong vertex-finding accuracy of $\delta r_{V_{\parallel(\perp)}}$ = 240.0 (24.) μm for the direction along (perpendicular to) the resultant vertex flight direction. The LAC energy resolution is estimated to be $\frac{\sigma_E}{E} \approx 0.65/\sqrt{E(\text{ GeV})}$ [18] for hadronic showers and $\approx 0.15/\sqrt{E(\text{ GeV})}$ [19] for electromagnetic showers. Muon identification is provided by the WIC, while electron identification utilizes CDC tracks and calorimeter clusters [20]. For muons of momentum $p > 3$ GeV and in the polar angle range $|\cos\theta| < 0.6$ the identification efficiency is 85%, while for electrons the efficiency varies from 50% for all electrons to 75% for

those with high momentum and transverse momentum with respect to the nearest jet axis [21]. Muons and electrons selected in this analysis, namely those which have transverse momentum with respect to the nearest jet axis greater than 1.0 GeV, are identified with purities of 99% and 75%, respectively.

The trigger and initial selection of hadronic events is described in [22]. A set of cuts was applied to the data to select well-measured tracks and events well-contained within the detector acceptance. Charged tracks were required to have (i) a closest approach transverse to the beam axis within 5 cm, and within 10 cm along the axis from the measured interaction point; (ii) a polar angle θ within $|\cos\theta| < 0.80$; and (iii) a momentum transverse to the beam axis, $p_\perp$ > 0.150 GeV/c. Events were required to have (i) a minimum of seven such tracks; (ii) a thrust axis [23] polar angle θ_T within $|cos\theta_T| < 0.71$; and (iii) a total visible energy E_{vis} of at least 20 GeV, which was calculated from the selected tracks assigned the charged pion mass.

The efficiency for selecting hadronic events satisfying the $|\cos\theta_T|$ cut was estimated to be above 96%. The background in the selected event sample was estimated to be 0.1 $\pm$ 0.1%, dominated by $Z^0 \to \tau^+\tau^-$ events. For our Monte Carlo (MC) study the JETSET7.4 [24] event generator was used, with parameter values tuned to hadronic e^+e^- annihilation data [25], combined with a simulation of B-decays tuned to $\Upsilon(4S)$ data [26] and a simulation of the SLD. Distributions of single particle and event topology observable in the selected events were found to be well-described by the simulation [27].

3 B Hadron Selection

We first applied a jet-finding algorithm to define a jet topology of each event. We used the JADE algorithm [28] with y_c = 0.02. To identify jets containing semileptonically-decaying B hadrons we considered jets containing an identified muon or electron with a transverse momentum $p_\perp^l$ of at least 1 GeV/c with respect to the nearest jet axis.

Figure 1 shows the lepton $p_\perp^l$ distribution in the data compared with the MC simulation in which the origin of the leptons is indicated. The efficiency for this selection to correctly identify the lepton in jets containing true $B \to D l X$ decays was estimated from the MC simulation to be 38% and the purity of the selected jet sample was estimated to be 72%. The purity was improved by the addition of D vertex information, as described below.

In each selected jet we then searched for a secondary D vertex comprised of tracks whose 3D impact parameter was inconsistent with the IP by at least 1σ. Two-prong vertex candidates were formed from all pairs of such tracks satisfying the following requirements: the momentum of the track was required to be in the range $0.150 < p < 55.0$ GeV/c; the distance of closest approach in the radial and axial directions was required to be less than 1 cm to remove background from K_s^0 decays and γ conversions; the track was required to be well-contained in the CDC, with $|\cos\theta| \leq 0.70$, have at least 40 hits in the CDC and to be well-linked to hits in the VXD, If the distance-of-closest-approach of the two tracks was less than 0.012 cm the pair was fitted to a common vertex and the vector $\vec{r}$ from the IP to the fitted vertex position was calculated in 3D. Two-prong vertices were then required to have: a χ^2 value for the vertex fit < 5; an invariant mass of the pair of tracks, m_D, consistent with a D hadron, $0.3 < m_D < 1.9$ GeV/c^2; and an invariant mass including the lepton, m_B, less than the B hadron mass, $m_B < 4.5$ GeV/c^2. The resultant D flight distance was required to make a projection onto the jet axis $r_D \geq 0.05$ cm, and this quantity normalized by its error r_D/σ_{r_D} was required to be greater than unity. If the distance-of-closest-approach between the resultant D momentum and the lepton momentum was less than 0.012 cm, a vertex fit of these momenta was made as a measure of the B vertex position. The distance from this position to the D vertex position, projected onto the D momentum vector was required to exceed 0.025 cm, and this quantity normalized by its error was required to exceed unity. Higher-prong vertices were formed if two or more 2-prong vertices were found, in which case an effective vertex was taken to contain all the

relevant tracks. From our data sample collected in the 1993 and 1994/1995 runs, 505 events contained at least one selected vertex and a selected lepton. The distribution of the number of tracks per vertex for these events is shown in Figure 2.

The purity of the final semileptonic B sample was defined to be the fraction of the tagged events whose identified leptons l are from $B \rightarrow DlX$, and was estimated from the MC simulation to be 84.5%. A further 12% of the selected events contain B decays with a cascade, punch-through or mis-identified lepton, and are still useful. The remaining 3.5% are non-$b\bar{b}$ events. For the 84.5% of tagged events with the desired topology, we list in Table 1 the efficiencies for selecting vertices from the different charmed species. Further, in this sample, we identify "true" vertices to be those vertices whose original two candidate tracks both originate from a D decay, and "fake" vertices to be those in which one or more of the tracks is not from a D. We define the purity Π as the number of true vertices divided by the total number of found vertices, and list it also in Table 1 along with the D hadron origin of selected vertices in the sample.

4 Measurement of the B Energies

We then proceeded to reconstruct the B hadron energy E_B^{Rec} according to

$$E_B^{Rec} = E_b - E_{frag}, \tag{1}$$

where E_b is the energy of the jet containing the B hadron and E_{frag} is the total energy in the jet not attributed to the B. E_{frag} is the sum of the charged and neutral components, E_{frag}^{chg} and E_{frag}^{neu}, respectively. E_{frag}^{chg} is the sum of the energy, using the momentum and assuming the pion mass, of all the charged tracks in the jet, not counting the lepton and the vertex tracks. E_{frag}^{neu} is the sum of the energy of calorimeter clusters in the jet that are not associated to charged tracks, The cluster energy scale was calibrated from studies of $\pi^0 \rightarrow \gamma\gamma$ in the data [18]. For 2-jet events the event was divided into two hemispheres by the plane perpendicular to the thrust, axis, and E_{frag} was calculated for the hemisphere containing the B hadron candidate. For 3-jet events we

corrected the jet energies according to the angles between the jet axes and assuming overall energy and momentum conservation in each event. Labeling the jets 1,2 and 3 and the angles between them θ_{23}, θ_{13} and θ_{12}, the corrected energy of jet 1 is given by $E_1 = \sqrt{s}(\sin\theta_{23})/(\sin\theta_{12} + \sin\theta_{23} + \sin\theta_{13})$, with corresponding expressions for jets 2 and 3. This procedure is described in more detail in reference [29], and results in improved jet energy resolution. E_{frag} was then calculated for the jet containing the B. For the JADE algorithm and y_c value used, approximately 9% of the selected events were classified as 4-jet states. Since for the 4-jet topology the jet energy correction technique is not applicable, we treated the 4-jet events in the same manner as the 2-jet events.

We note that the JETSET7.4 event generator used in our MC simulation does not produce orbitally-excited B** mesons, and there is now evidence for their production in Z^0 decays [30]. We corrected our simulation to account for them. For 20.7% of all B hadrons in our simulation, we adjusted the energy E_B^{True} to $E_B^{True} + E_\pi$, where the pion energy E_π was produced according to an isotropic 2-body decay distribution for $B^{**} \rightarrow B\pi^{\pm}$, assuming a B** mass of 5.7 GeV/c^2.

Figure 3 shows a MC simulation of the correlations between the reconstructed and true values of E_{frag}^{chg} and E_{frag}^{neu}. We studied the dependence of the correlations on thrust axis polar angle and found consistent. results over the range $|\cos\theta_T| \leq 0.71$. A second-order polynomial was fitted to the E_{frag}^{neu} correlation plot and was used to correct. this quantity for each jet measured in the data. The resulting distribution of E_B^{Rec} is shown for the data in Figure 4. A cross-check on jet axis modeling, made by varying y_c in the range $0.005 \leq y_c \leq 0.02$ and repeating the analysis, also yielded consistent results. Also shown in Figure 4 is the expected contribution from all non-B $\rightarrow Dl X$ events, as estimated from the MC simulation.

Figure 5 shows a histogram of $(E_B^{True} - E_B^{Rec})/E_B^{True}$ for the simulated events, compared with a 2-Gaussian fit, the peak positions of which were constrained to be equal. The small tails, narrow inner core and asymmetric shape are features of this analysis.

The 2-Gaussian fit yields a core containing 96% of the events with a $\pm 10\%$ resolution.

5 Correction of the B Energy Distribution

The measured B energy distribution must be corrected for background contributions, acceptance effects, the effects of missing or extra tracks in a reconstructed D vertex, extra neutral energy from D* and D** production, and the effects of misassigned extra tracks and clusters in jets. These effects can cause bin-to-bin migrations between the true and reconstructed distributions.

To obtain the normalized distribution of x_E, labeled $\mathbf{D}^{\mathbf{data}}_{\mathbf{True}}$, we performed a full matrix unfolding procedure to the normalized distribution of E_B^{Rec}, labeled $\mathbf{D}^{\mathbf{data}}_{\mathbf{Rec}}$:

$$\mathbf{D}^{\mathbf{data}}_{\mathbf{True}} = \boldsymbol{\epsilon} \cdot \mathbf{E} \cdot \mathbf{S} \cdot \mathbf{D}^{\mathbf{data}}_{\mathbf{Rec}}, \tag{2}$$

where $\boldsymbol{\epsilon}$ is the diagonal matrix comprising the acceptance correction, **S** is a diagonal matrix comprising the background subtraction, and **E** is a non-diagonal unfolding matrix. A similar equation can be constructed for the MC simulated events, with $\mathbf{D}^{\mathbf{MC}}_{\mathbf{True}}$ and $\mathbf{D}^{\mathbf{MC}}_{\mathbf{Rec}}$ the true and reconstructed normalized, scaled E_B^{True} and E_B^{Rec} distributions. respectively:

$$\mathbf{D}^{\mathbf{MC}}_{\mathbf{True}} = \boldsymbol{\epsilon} \cdot \mathbf{E} \cdot \mathbf{S} \cdot \mathbf{D}^{\mathbf{MC}}_{\mathbf{Rec}}. \tag{3}$$

$\boldsymbol{\epsilon}$ and **S** were determined from the MC simulation, and an iterative procedure [2] using equations 2 and 3, was used to calculate **E.** We used 12 energy bins.

The calculation of **E** is problematic, in that it depends on the shape and parameters of the assumed input *b* fragmentation function in the MC simulation. We therefore adopted the following iterative procedure for investigating the shape-dependence of the unfolding matrix **E.** We chose a particular function and fitted it to the data distribution of E_B^{Rec}, using MINUIT [31] to minimize the χ^2, where the error in each bin was taken to be the square root of the expected number of entries in that bin. At the zero^{th} iteration **E** was taken to be the unit matrix **1,** and $\mathbf{D}^{\mathbf{data}}_{\mathbf{True}}$ was evaluated and used as

the MC input $\mathbf{D}_{\mathbf{True}}^{\mathbf{MC}}$. **E** was then constructed event-by-event on the right-hand-side of equation 3 and inserted in equation 2 to re-derive $\mathbf{D}_{\mathbf{True}}^{\mathbf{data}}$. Throughout, we used universal $\boldsymbol{\epsilon}$ and **S.** The iteration was repeated until the value of $\mathbf{D}_{\mathbf{True}}^{\mathbf{data}}$ in each bin changed by less than $\pm 10\%$ from its value at the previous iteration.

The final unfolded $\mathbf{D}_{\mathbf{True}}^{\mathbf{data}}$ depends on the function chosen for this process. We used five functions, a third-order polynomial and four functions resulting from models of the heavy quark fragmentation†. Table 2 shows the forms of the functions used along with their χ^2 values for the fit to $\mathbf{D}_{\mathbf{Rec}}^{\mathbf{data}}$ at the initial and final iterations. The value of $\langle x_E \rangle$ and the parameters of the fit at the final iteration are also shown for each function, with their errors. The final χ^2/dof values are small due to the fact that. the iterative procedure drives the unfolded data to resemble the function used to calculate **E.**

Figure 6 shows $\mathbf{D}_{\mathbf{True}}^{\mathbf{data}}$ at the last iteration, derived using the functions listed in Table 2. In contrast to [2], functions were not omitted from considerate ion because their fit to $\mathbf{D}_{\mathbf{Rec}}^{\mathbf{data}}$ at the zeroth iteration yielded poor χ^2 values. We verified that this procedure was able to reproduce, to within statistical errors, fragmentation functions from toy Monte Carlo models with a wide range of input $\langle x_E \rangle$. The final matrix ρ indicating the degree of correlation among the statistical errors is shown in Table 3.

6 Systematic Errors and Average x_E

To calculate the systematic errors in each of the 12 bins of the x_E distribution we constructed new $\boldsymbol{\epsilon}$ and **S** matrices for each systematic effect under consideration and repeated the iterative procedure to re-derive $\mathbf{D}_{\mathbf{True}}^{\mathbf{data}}$. Sources of error were divided into detector modeling errors and physics modeling errors, where the latter category included the function-dependent unfolding uncertainty, as well as errors due to uncertainties on experimental measurements serving as input parameters to the underlying physics modeling. Most of the physics modeling errors were handled with a re-weighting

†The phenomenological functions are functions of the experimentally inaccessible variable z = $(E + p_{\parallel})_{hadron}/(E + p)_{quark}$, though we use them here in terms of x_E.

technique, where events were weighted according to the new likelihood with which they may occur.

The neutral fragmentation energy E_{frag}^{neu} measurement was found to be the main source of detector modeling error. The neutral energy measurement uncertainty was estimated by varying the fit parameters of the fitted correlation between the true and reconstructed neutral fragmentation energies within their errors.

For the physics modeling errors, we varied several parameters that are described in detail in [19] and [32]. The central values and range of variation are listed in Table 4. The resulting uncertainty on the contents of the individual bins of $\mathbf{D}_{\mathbf{True}}^{\mathbf{data}}$ was taken as the quadrature sum in that bin of all of the variations from all the physics systematic errors in Table 4. The uncertainty on $\langle x_E \rangle$ from each of these sources is listed in Table 4.

The function-dependent unfolding uncertainty was estimated by repeating t he analysis separately with each of the trial functions. The central value for each bin in the unfolded x_E distribution was defined using the Peterson function, and the error due to the choice of trial function was taken as the extrema of the content in that bin using the five functions. The distribution $\mathbf{D}_{\mathbf{True}}^{\mathbf{data}}$ is shown in Figure 7. In each bin the statistical error, the unfolding error, and the total systematic error are indicated; note that the unfolding error is typically the largest uncertainty.

The mean scaled energy $\langle x_E \rangle = \sum_{i=1}^{12} (x_i \cdot D_{True,i}^{data})$, where x_i is the center of bin i and $D_{True,i}^{data}$ is the normalized content of bin i, was calculated using in turn each of the five functions in the iterative procedure described above. We chose the $\langle x_E \rangle$ derived using the Peterson function as our central value, and the error due to the choice of trial functions was taken from the extrema in $\langle x_E \rangle$. We note that although the functions used in the unfolding yield different $\mathbf{D}_{\mathbf{True}}^{\mathbf{data}}$, the value of $\langle x_E \rangle$ was not found to be sensitive to the choice of function (Table 2). The leading contribution to the error $\left(^{+3.16}_{-1.64}\%\right)$ comes from our uncertainty on the measurement of the neutral fragmentation energy.

It is interesting to investigate how well the phenomenological models can parametrize our $\mathbf{D}^{\mathbf{data}}_{\mathbf{True}}$. We generated MC simulations for three particular models at several parameter values. We also ran a program provided by P. Nason with parameters taken from reference [6]. We find that all models are able to describe the data. Figure 8 shows examples of these four theoretical models overlaid on our final $\mathbf{D}^{\mathbf{data}}_{\mathbf{True}}$. Table 5 shows the parameters and χ^2s of the plotted Bowler, BCY and Peterson functions along with the parameter set for the Nason/Colangelo/Mele function.

7 Summary and Conclusions

Using the high-precision SLD tracking system to find secondary vertices, we have measured the *b* quark fragmentation function in e^+e^- annihilation at the Z^0 resonance from a sample of semileptonically-decaying B hadrons. We reconstructed the B energy event-by-event using the information from the lepton, a D hadron vertex, and energy conservation. We reconstructed the energy of 96% of the tagged B hadrons with a FWHM resolution of 10%.

We used an iterative procedure to unfold the measured fragmentation function to the true one. We compared the fragmentation function with the predictions of several models, in each case applying a consistent treatment of the data correction procedure. We found that all models considered were able to describe the data. We report an average value of the scaled primary B energy in Z^0 decays of

$$\langle x_E \rangle = 0.697 + 0.012(stat)^{+0.028}_{-0.024}(syst). \quad \text{(PRELIMINARY)}$$

Figure 9 shows this result in comparison with measurements from other experiments.

Acknowledgments

We thank the personnel of the SLAC accelerator department and the technical staffs of our collaborating institutions for their outstanding efforts on our behalf.

References

[1] ALEPH Collab., D. Buskulic *et al., Z.* Phys. **C62** (1994) 179.
DELPHI Collab., P. Abreu *et al.,* CERN-PPE/95-08 (1995).
L3 Collab., O. Adeva *et al.,* Phys Lett. **B261** (1991) 177.
OPAL Collab., P.D, Acton *et al.,* Z. Phys, **C60** (1993) 199.

[2] ALEPH Collab., D. Buskulic *et al,,* Phys. Lett. **B357** (1995) 699.

[3] OPAL Collab., P.D. Acton *et al.,* CERN-PPE/95-122 (1995).

[4] DELPHI Collab., P. Abreu *et al.,* CERN-PPE/95-076 (1995).

[5] V. Blobel, in Proceedings of the CERN School of Computing (1984) 88.

[6] B. Mele and P. Nason, Phys. Lett. **B245** (1990) 635.
B. Mele and P. Nason, Nucl. Phys. **B361** (1991) 626.
G. Colangelo and P. Nason, Phys. Lett. **B285** (1992) 167.

[7] E. Braaten, K. Cheung and T.C. Yuan, Phys. Rev. **D48** (1993) R5049.

[8] C. Peterson, D. Schlatter, 1. Schmitt and P.M. Zerwas, Phys. Rev. **D27** (1983) 105.

[9] B. Andersson, G. Gustafson, G. Ingelman, T. Sjöstrand, Phys. Rep. **97** (1983) 32.

[10] M.G. Bowler, Z. Phys. **C11** (1981) 169.

[11] See *e.g.* SLD Collab., K. Abe *et al.,* Phys. Rev. Lett. **75** (1993) 3624.
OPAL Collab., P. Acton *et al., Z.* Phys. **C61** (1994) 201.
SLD Collab., K. Abe *et al.,* SLAC-PUB-7172 (1996).

[12] ALEPH Collab., D. Buskulic *et al.,* CERN PPE-95-084 (1995).
SLD Collab., K. Abe *et al.,* SLAC-PUB-7067, (1995).

[13] SLD Design Report, SLAC. Report 273 (1984).

[14] M.D. Hildreth *et al.*, SLAC-PUB-6656 (1994), submitted to IEEE Trans. Nucl. Sci.

[15] C. J. S. Damerell *et al.*, Nucl. Inst. Meth. **A288** (1990) 288.

[16] D. Axen *et al.*, Nucl, Inst. Meth. **A328** (1993) 472.

[17] A. C. Benvenuti *et al.*, Nucl. Inst. Meth. **A290** (1990) 353.

[18] S. Gonzalez-Martirena, MIT Ph.D. Thesis, SLAC-Report-439 (1994).

[19] SLD Collab., K. Abe *et al.*, Phys. Rev. **D53** (1996) 1023.

[20] David C. Williams, MIT Ph.D. Thesis, SLAC-Report-445 (1994).

[21] SLD Collab., K. Abe *et al.*, SLAC-PUB-6607 (1994).

[22] SLD Collab., K. Abe *et al.*, Phys. Rev. Lett. **73** (1994) 25.

[23] S. Brandt *et al.*, Phys. Lett. **12** (1964) 57.
E. Farhi, Phys. Rev. Lett. **39** (1977) 1587.

[24] T. Sjöstrand, CERN-TH.7112/93 (1993).

[25] P. N. Burrows, Z. Phys. **C41** (1988) 375.
OPAL Collab., M.Z. Akrawy *et al.*, Z. Phys. **C47** (1990) 505.

[26] SLD Collab., K. Abe *et al.*, Phys. Rev. **D53** (1996) 1023.

[27] SLD Collaboration, K. Abe *et al.*, Phys. Rev, **D51** (1995) 962.

[28] W. Bartel *et al.*, Z. Phys. **C33** (1986) 23.

[29] SLD Collab., K. Abe *et al.*, SLAC-PUB-7099 (1996); submitted to Phys. Rev. D.

[30] OPAL Collab., PD. Acton *et al.*, Z. Phys. **C66** (1995) 19.
DELPHI Collab., P. Abreu *et al.*, Phys. Lett. **B345** (1995) 598.
ALEPH Collab., D. Buskulic *et al.*, CERN-PPE/95-108 (1995).

[31] F. James and M. Roos, CERN-D506 (1989).

[32] SLD Collab., K. Abe *et al.*, SLAC-PUB-6972 (1995).

[33] ALEPH Collab., D. Buskulic *et al.*, Z. Phys, **C62** (1994) 179.
ALEPH Collab., D. Buskulic *et al.*, Phys. Lett. **B244** (1990) 551.
OPAL Collab., P.D. Acton *et al.*, Z. Phys. **C61** (1994) 219.
OPAL Collab., P.D. Acton *et al.*, Z. Phys. **C58** (1993) 523.
DELPHI Collab., P. Abreu *et al.*, Z. Phys. **C57** (1993) 181.
L3 Collab., O. Adeva *et al.*, Phys. Lett. **B241** (1990) 416.
L3 Collab., O. Adeva *et al.*, Phys. Lett. **B261** (1991) 177.

** K. Abe,[19] K. Abe,[29] I. Abt,[13] T. Akagi,[27] N.J. Allen,[4] W.W. Ash,[27]†
D. Aston,[27] K.G. Baird,[24] C. Baltay,[33] H.R. Band,[32] M.B. Barakat,[33]
G. Baranko,[9] O. Bardon,[15] T. Barklow,[27] A.O. Bazarko,[10] R. Ben-David,[33]
A.C. Benvenuti,[2] G.M. Bilei,[22] D. Bisello,[21] G. Blaylock,[6] J.R. Bogart,[27]
B. Bolen,[17] T. Bolton,[10] G.R. Bower,[27] J.E. Brau,[20] M. Breidenbach,[27]
W.M. Bugg,[28] D. Burke,[27] T.H. Burnett,[31] P.N. Burrows,[15] W. Busza,[15]
A. Calcaterra,[12] D.O. Caldwell,[5] D. Calloway,[27] B. Camanzi,[11] M. Carpinelli,[23]
R. Cassell,[27] R. Castaldi,[23][a] A. Castro,[21] M. Cavalli-Sforza,[6] A. Chou,[27]
E. Church,[31] H.O. Cohn,[28] J.A. Coller,[3] V. Cook,[31] R. Cotton,[4]
R.F. Cowan,[15] D.G. Coyne,[6] G. Crawford,[27] A. D'Oliveira,[7] C.J.S. Damerell,[25]
M. Daoudi,[27] R. De Sangro,[12] R. Dell'Orso,[23] P.J. Dervan,[4] M. Dima,[8]
D.N. Dong,[15] P.Y.C. Du,[28] R. Dubois,[27] B.I. Eisenstein,[13] R. Elia,[27]
E. Etzion,[4] D. Falciai,[22] C. Fan,[9] M.J. Fero,[15] R. Frey,[20] K. Furuno,[20]
T. Gillman,[25] G. Gladding,[13] S. Gonzalez,[15] G.D. Hallewell,[27] E.L. Hart,[28]
J.L. Harton,[8] A. Hasan,[4] Y. Hasegawa,[29] K. Hasuko,[29] S. J. Hedges,[3]
S.S. Hertzbach,[16] M.D. Hildreth,[27] J. Huber,[20] M.E. Huffer,[27] E.W. Hughes,[27]

H. Hwang,[20] Y. Iwasaki,[29] D.J. Jackson,[25] P. Jacques,[24] J. A. Jaros,[27]
A.S. Johnson,[3] J.R. Johnson,[32] R.A. Johnson,[7] T. Junk,[27] R. Kajikawa,[19]
M. Kalelkar,[24] H. J. Kang,[26] I. Karliner,[13] H. Kawahara,[27] H.W. Kendall,[15]
Y. D. Kim,[26] M.E. King,[27] R. King,[27] R.R. Kofler,[16] N.M. Krishna,[9]
R.S. Kroeger,[17] J.F. Labs,[27] M. Langston,[20] A. Lath,[15] J.A. Lauber,[9]
D.W.G.S. Leith,[27] V. Lia,[15] M.X. Liu,[33] X. Liu,[6] M. Loreti,[21] A. Lu,[5]
H.L. Lynch,[27] J. Ma,[31] G. Mancinelli,[22] S. Manly,[33] G. Mantovani,[22]
T.W. Markiewicz,[27] T. Maruyama,[27] H. Masuda,[27] E. Mazzucato,[11]
A.K. McKemey,[4] B.T. Meadows,[7] R. Messner,[27] P.M. Mockett,[31]
K.C. Moffeit,[27] T.B. Moore,[33] D. Muller,[27] T. Nagamine,[27] S. Narita,[29]
U. Nauenberg,[9] H. Neal,[27] M. Nussbaum,[7] Y. Ohnishi,[19] L.S. Osborne,[15]
R.S. Panvini,[30] H. Park,[20] T.J. Pavel,[27] I. Peruzzi,[12][b] M. Piccolo,[12]
L. Piemontese,[11] E. Pieroni,[23] K.T. Pitts,[20] R.J. Plano,[24] R. Prepost,[32]
C.Y. Prescott,[27] G.D. Punkar,[27] J. Quigley,[15] B.N. Ratcliff,[27] T.W. Reeves,[30]
J. Reidy,[17] P.E. Rensing,[27] L.S. Rochester,[27] P.C. Rowson,[10] J.J. Russell,[27]
O.H. Saxton,[27] T. Schalk,[6] R.H. Schindler,[27] B.A. Schumm,[14] S. Sen,[33]
V.V. Serbo,[32] M.H. Shaevitz,[10] J.T. Shank,[3] G. Shapiro,[14] D.J. Sherden,[27]
K.D. Shmakov,[28] C. Simopoulos,[27] N.B. Sinev,[20] S.R. Smith,[27] M.B. Smy,[8]
J.A. Snyder,[33] P. Stamer,[24] H. Steiner,[14] R. Steiner,[1] M.G. Strauss,[16] D. Su,[27]
F. Suekane,[29] A. Sugiyama,[19] S. Suzuki,[19] M. Swartz,[27] A. Szumilo,[31]
T. Takahashi,[27] F.E. Taylor,[15] E. Torrence,[15] A.I. Trandafir,[16] J.D. Turk,[33]
T. Usher,[27] J. Va'vra,[27] C. Vannini,[23] E. Vella,[27] J.P. Venuti,[30] R. Verdier,[15]
P.G. Verdini,[23] S.R. Wagner,[27] A.P. Waite,[27] S.J. Watts,[4] A.W. Weidemann,[28]
E.R. Weiss,[31] J.S. Whitaker,[3] S.L. White,[28] F.J. Wickens,[25] D.A. Williams,[6]
D.C. Williams,[15] S.H. Williams,[27] S. Willocq,[33] R.J. Wilson,[8]
W.J. Wisniewski,[27] M. Woods,[27] G.B. Word,[24] J. Wyss,[21] R.K. Yamamoto,[15]
J.M. Yamartino,[15] X. Yang,[20] S.J. Yellin,[5] C.C. Young,[27] H. Yuta,[29]
G. Zapalac,[32] R.W. Zdarko,[27] C. Zeitlin,[20] and J. Zhou,[20]

[1] *Adelphi University, Garden City, New York 11530*

[2] *INFN Sezione di Bologna, I-40126 Bologna, Italy*

[3] *Boston University, Boston, Massachusetts 02215*

[4] *Brunel University, Uxbridge, Middlesex UB8 3PH, United Kingdom*

[5] *University of California at Santa Barbara, Santa Barbara, California 93106*

[6] *University of California at Santa Cruz, Santa Cruz, California 95064*

[7] *University of Cincinnati, Cincinnati, Ohio 45221*

[8] *Colorado State University, Fort Collins, Colorado 80523*

[9] *University of Colorado, Boulder, Colorado 80309*

[10] *Columbia University, New York, New York 10027*

[11] *INFN Sezione di Ferrara and Università di Ferrara, I-44100 Ferrara, Italy*

[12] *INFN Lab. Nazionali di Frascati, I-00044 Frascati, Italy*

[13] *University of Illinois, Urbana, Illinois 61801*

[14] *Lawrence Berkeley Laboratory, University of California, Berkeley, California 94720*

[15] *Massachusetts Institute of Technology, Cambridge, Massachusetts 02139*

[16] *University of Massachusetts, Amherst, Massachusetts 01003*

[17] *University of Mississippi, University, Mississippi 38677*

[19] *Nagoya University, Chikusa-ku, Nagoya 464 Japan*

[20] *University of Oregon, Eugene, Oregon 97403*

[21] *INFN Sezione di Padova and Università di Padova, I-35100 Padova, Italy*

[22] *INFN Sezione di Perugia and Università di Perugia, I-06100 Perugia, Italy*

[23] *INFN Sezione di Pisa and Università di Pisa, I-56100 Pisa, Italy*

[24] *Rutgers University, Piscataway, New Jersey 08855*

[25] *Rutherford Appleton Laboratory, Chilton, Didcot, Oxon OX11 0QX United Kingdom*

[26] *Sogang University, Seoul, Korea*

[27] *Stanford Linear Accelerator Center, Stanford University, Stanford, California*

94309

[28] *University of Tennessee, Knoxville, Tennessee 37996*

[29] *Tohoku University, Sendai 980 Japan*

[30] *Vanderbilt University, Nashville, Tennessee 37235*

[31] *University of Washington, Seattle, Washington 98195*

[32] *University of Wisconsin, Madison, Wisconsin 53706*

[33] *Yale University, New Haven, Connecticut 06511*

† *Deceased*

[a] *Also at the Università di Genova*

[b] *Also at the Università di Perugia*

Charmed species	ϵ (%)	Π (%)	C (%)
D^0	47	95	67
D^+	39	96	18
D_s	47	99	10
Λ_c	19	92	5

Table 1: Efficiency ϵ and purity Π for selecting vertices from various D hadron types in events with a selected lepton from a B decay. The composition C of the sample of vertices is also shown. The MC statistical errors are less than δC = 2%, $\delta\epsilon$ = 1%, and $\delta\Pi$ = 2% for all cases.

Function Name	Functional. form	Reference
Peterson	$f(x) = N\frac{1}{x}(1 - \frac{1}{x} - \frac{\epsilon_b}{1-x})^{-2}$	[8]
Lund	$f(x) = N\frac{1}{x}(1-x)^a \exp(-bm_T^2/x)$	[9]
BCY	$f(x) = N\frac{r(1-2r)(2r)^2}{(1-(1-r)(1-2r))^6}[12 + \mathcal{O}(x^1) + \mathcal{O}(x^2) + \ldots]$	[7]
ALEPH	$f(x) = a\frac{1+b(1-x)}{x}(1 - \frac{c}{x} - \frac{d}{1-x})^{-2}$	[2]
3^{rd}-order Polynomial	$f(x) = a + bx + cx^2 + dx^3$	

Function name	χ^2_i	χ^2_f	Final fitted parameters	$\langle x_E \rangle = \frac{\int dx_E\, x_E\, f(x_E)}{\int dx_E\, f(x_E)}$
Peterson	33.0/10	2.4/10	$N = 0.0341 \pm 0.0016$	0.712
			$\epsilon_b = 0.0402 \pm 0.0022$	
Lund	157./9	0.9/9	$N = 9.803 \pm 0.452$	0.708
			$a = 0.786 \pm 0.031$	
			$b = 0.0876 \pm 0.0011$	
BCY	71./10	4.4/10	$N = 0.0493 \pm 0.0024$	0.691
			$r = 0.2308 \pm 0.0148$	
ALEPH	18.4/8	2.5/8	$a = (0.761 \pm 0.037) \cdot 10^{-3}$	0.721
			$b = 32.5 \pm 1.5$	
			$c = 0.841 \pm 0.0040$	
			$d = 0.0232 \pm 0.0008$	
3^{rd}-order polynomial	115./8	3.6/8	$a = 0.0432 \pm 0.0039$	0.677
			$b = -0.630 \pm 0.007$	
			$c = 2.27 \pm 0.01$	
			$d = -1.647 \pm 0.011$	

Table 2: Functions used in the iterative unfolding. Below, the χ^2s of their fits to $\mathbf{D}^{\mathbf{data}}_{\mathbf{True}}$ at the initial and final iteration. Also shown are the final fit parameters and final mean scaled energy $\langle x_E \rangle$ for the 5 functions.

	1	2	3	4	5	6	7	8	9	10	11	12
1	1.00	0.03	0.60	0.36	0.24	0.27	0.31	0.14	0.08	0.02	0.02	0.03
2		1.00	0.12	0.89	0.70	0.19	0.18	0.11	0.08	0.06	0.04	0.03
3			1.00	0.51	0.31	0.34	0.35	0.19	0.13	0.08	0.04	0.03
4				1.00	0.70	0.26	0.27	0.17	0.12	0.08	0.05	0.05
5					1.00	0.71	0.76	0.60	0.42	0.28	0.16	0.13
6						1.00	0.95	0.75	0.53	0.33	0.20	0.16
7							1.00	0.88	0.70	0.51	0.31	0.26
8								1.00	0.91	0.72	0.44	0.38
9									1.00	0.90	0.66	0.57
10										1.00	0.83	0.76
11											1.00	0.99
12												1.00

Table 3: The elements of the statistical correlation matrix $\rho_{ij} = V_{ij}/(\sigma_i \sigma_j)$, where the V_{ij} are the elements of the covariance matrix for bin *i* and *j* of $\mathbf{D}^{\mathbf{data}}_{\mathbf{True}}$.

	ERROR (%)
DETECTOR MODELING	
E_{frag}^{neu}	$^{+3.16}_{-1.64}$
PHYSICS MODELING	
Choice of Fitting Function	$^{+1.14}_{-2.27}$
B-lifetimes	
($\tau_{Bmeson} = 1.55 \pm 0.10$ ps,	$^{+0.25}_{-0.03}$
$\tau_{Bbaryon} = 1.10 \pm 0.30$ ps)	
$\mathbf{f_{B^{**}}}$ ($20.7 \pm 7\%$)	$^{+0.31}_{-0.31}$
$\mathbf{m_{B^{**}}}$ (5.704 ± 0.020 GeV)	$^{+0.27}_{-0.29}$
$\Gamma(B \rightarrow \mathbf{D^*})/\Gamma(B \rightarrow \mathbf{D})$ $(3-1)$	± 0.34
$\Gamma(B \rightarrow \mathbf{D^{**}})/\Gamma(B \rightarrow \mathbf{D})$ (3 ± 1)	$^{+0.12}_{-0.32}$
$\mathbf{B_u, B_d, B_s, \Lambda_b}$ **production**	
($40.1 \pm 20\%$,$40.1 \pm 20\%$,$11.6 \pm 8.0\%$,$8.9 \pm 8.0\%$)	$^{+0.31}_{-0.28}$
$\mathbf{B_u, B_d, B_s, \Lambda_b}$ **decay (6 modes each** $\pm 1\sigma$)	$^{+0.15}_{-0.11}$
B-decay multiplicity (± 0.25 **tracks per B decay**)	$^{+0.32}_{-0.20}$
c-**fragmentation**	
(Peterson $\langle x_E \rangle$ for $\mathrm{D^*} = 0.501 \pm 0.025$)	± 0.02
$\mathbf{D^0, D^+, D_s, \Lambda_c}$ **production**	
($56.0 \pm 5.3\%$,$23.0 \pm 3.7\%$,$12.0 \pm 7.0\%$,$8.9 \pm 0.5\%$)	± 0.03
c **decay multiplicity** ($\delta n_{D^0,D^+,D_s,\Lambda_c} = 6, 10, 31, 40\%$)	$^{+0.00}_{-0.02}$
s **production** ($s\bar{s}$ **popping varied by 10%**)	$^{+0.28}_{-0.26}$
R_b(± 0.003)	$^{+0.00}_{-0.03}$
R_c(± 0.02)	± 0.05
$g \rightarrow b\bar{b}$ **splitting**($\pm 50\%$)	$^{+1.22}_{-0.39}$
$g \rightarrow c\bar{c}$ **splitting**($\pm 50\%$)	± 0.15
Sub-total	$^{+1.87}_{-2.50}$
TOTAL	$^{+3.67}_{-2.99}$

Table 4: Systematic errors on $\langle x_E \rangle$.

Name	Parameters	χ^2/dof
Peterson	ϵ_b = 0.066	11.1/10
Bowler	r_b = 0.86, a = 0.18, b = 0.34	17.0/10
BCY	r = 2.105	20.2/10
Nason/Colangelo/Mele	Λ_5 = 200 MeV, $\mu = m_b$ = 4.5 GeV α_{np} = 0.595, β_{np} = 18.67	

Table 5: Parameters and χ^2 values, where the error in each bin was taken to be the square root of the expected number of entries in that bin, for the curves shown in Figure 8.

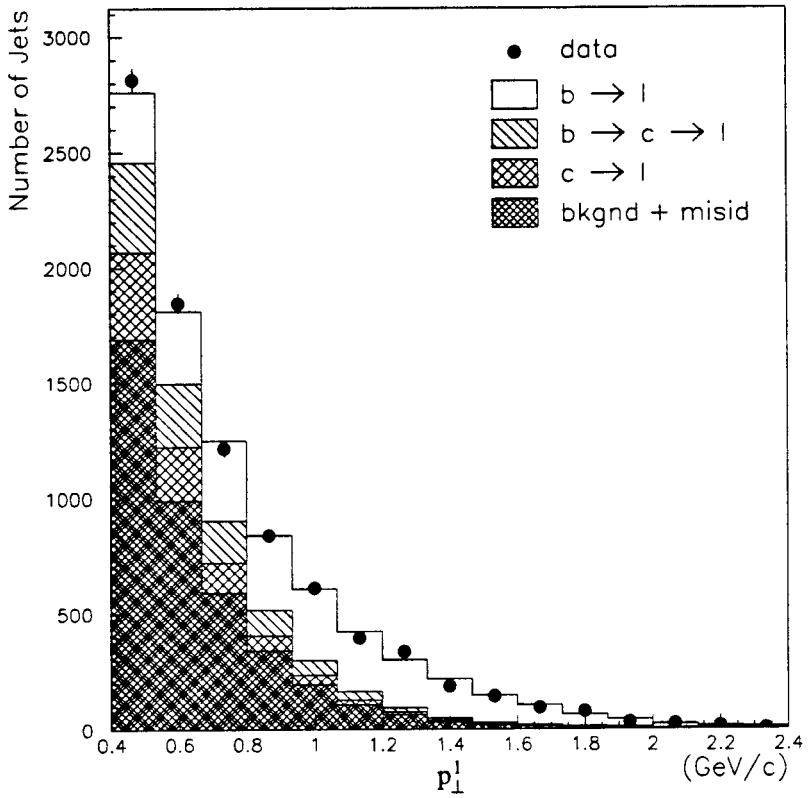

Figure 1: Distribution of lepton transverse momentum $p_\perp^l$ with respect to the closest jet axis for leptons with momentum $p > 4.0$ GeV/c.

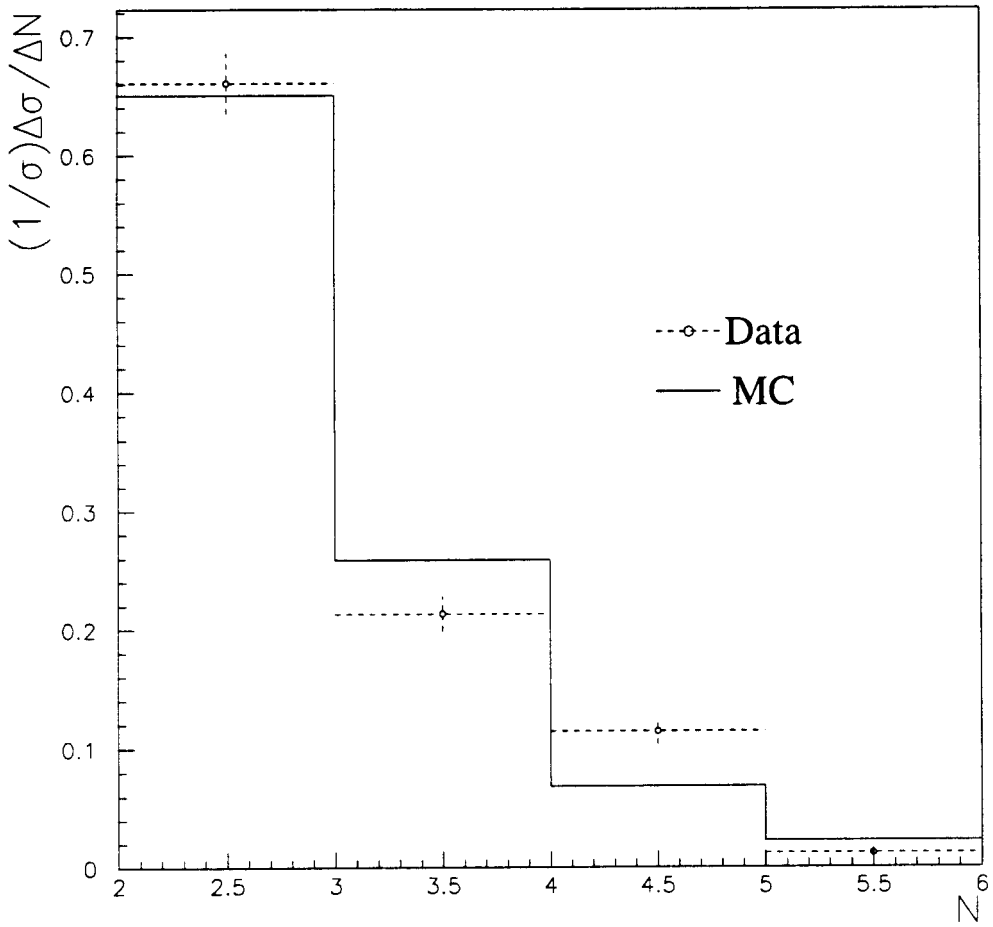

Figure 2: Distribution of the number of tracks in selected D vertices.

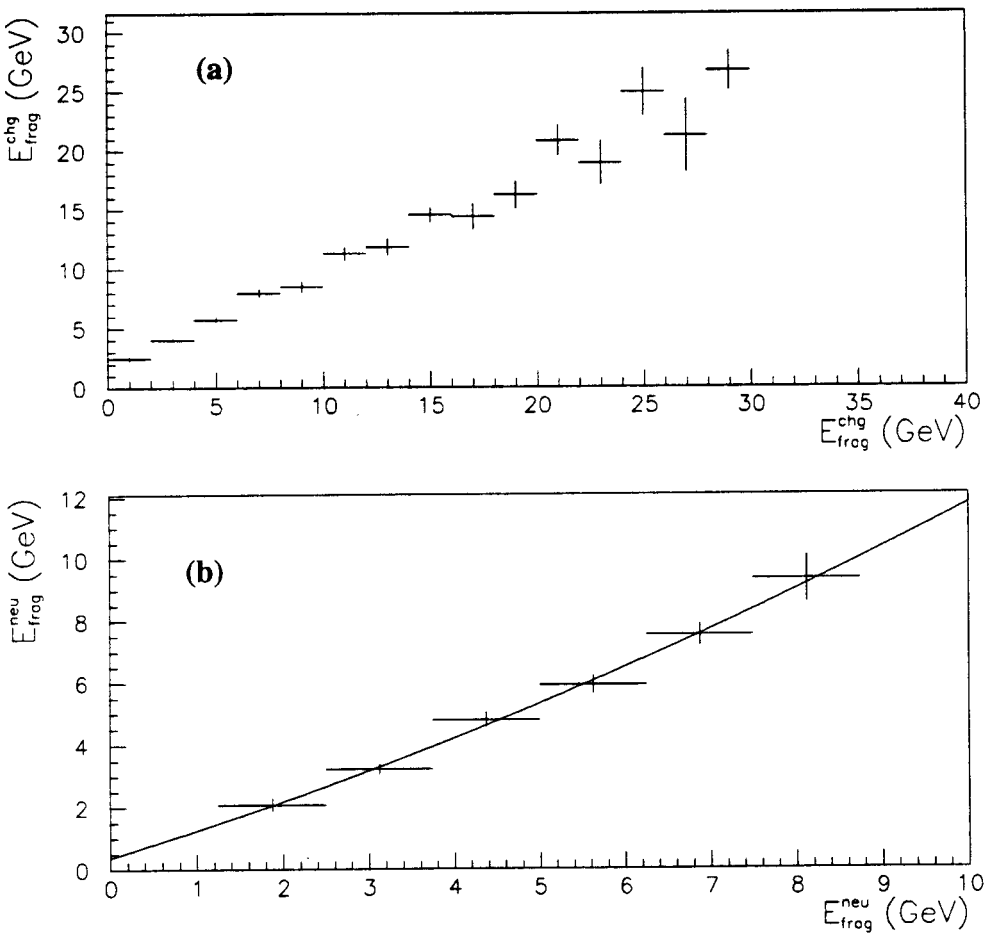

Figure 3: MC simulation of true vs. reconstructed (a) charged and (b) neutral fragmentation energy (see text). The 2^{nd}-order polynomial fit in (b) is used to obtain the neutral contribution to the fragmentation energy.

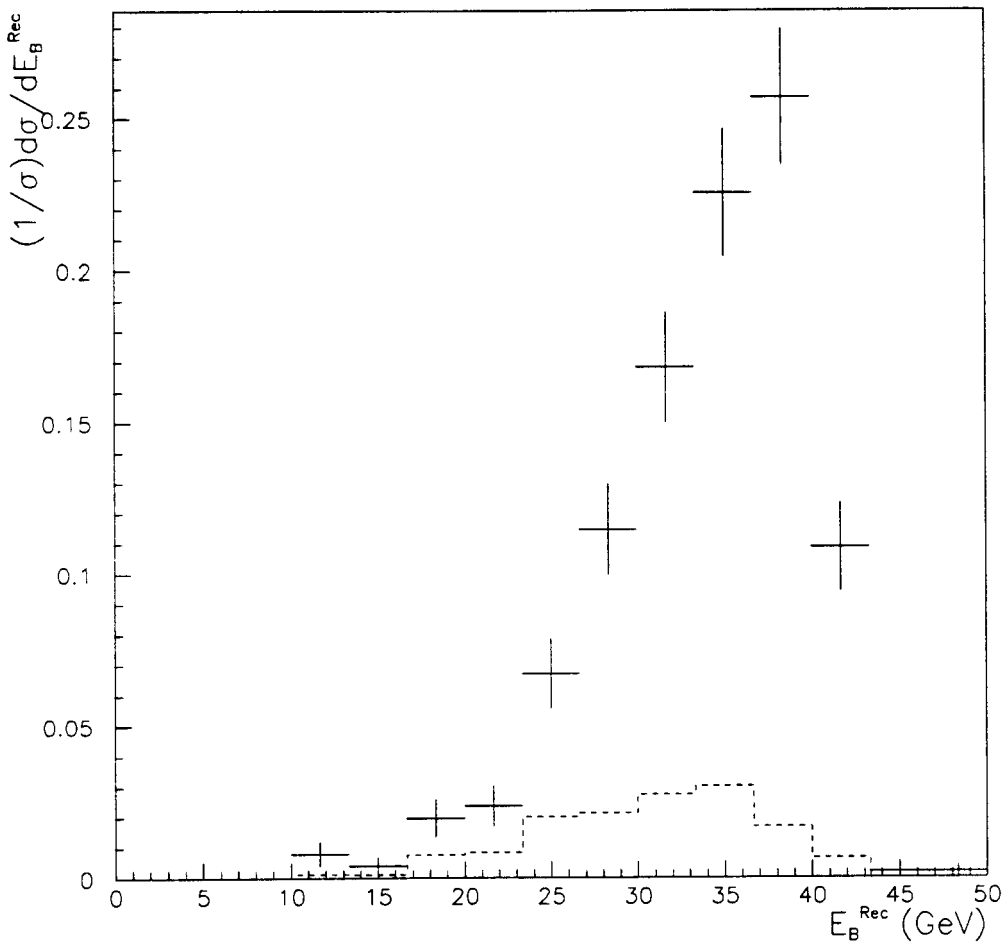

Figure 4: Distribution of E_B^{Rec} for the data. Estimated background is indicated by the dashed line.

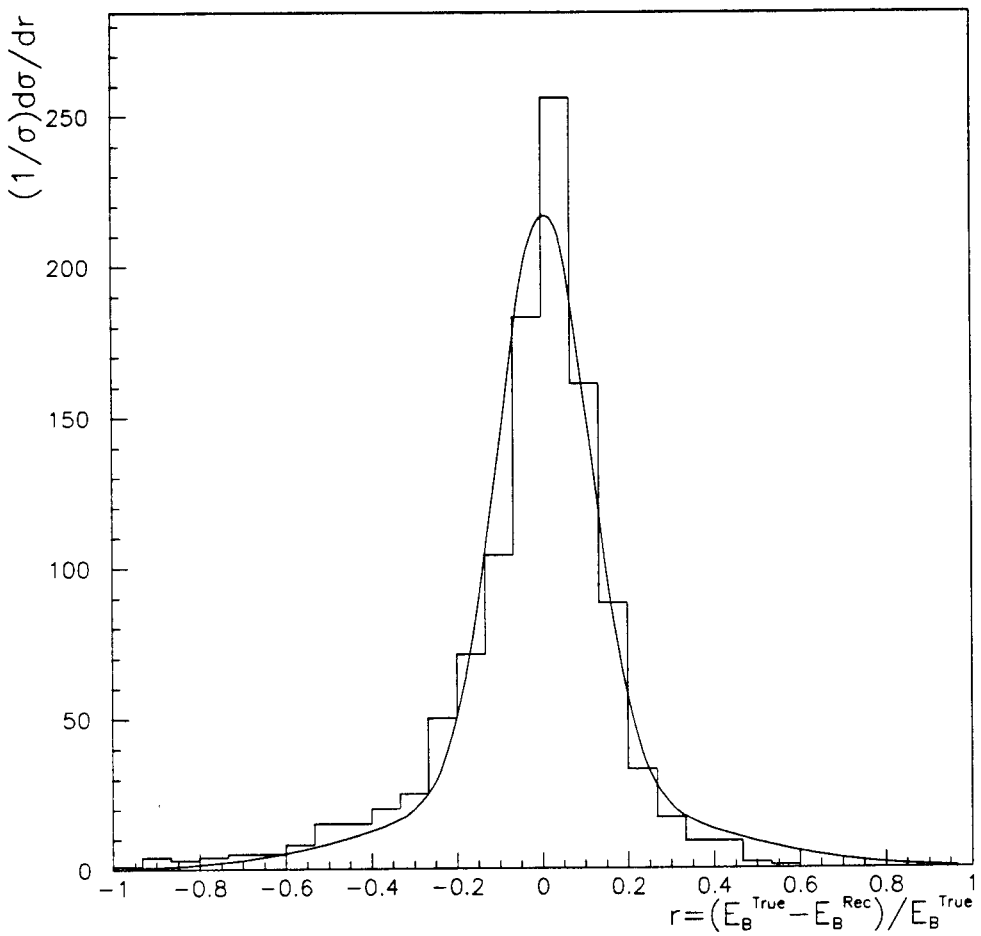

Figure 5: Normalised difference between the true and reconstructed B energies from the MC simulation. A fit is shown of 2 Gaussian distributions. The narrow Gaussian has a FWHM of r = 0.20 and contains 96% of the area enclosed by the fitted function.

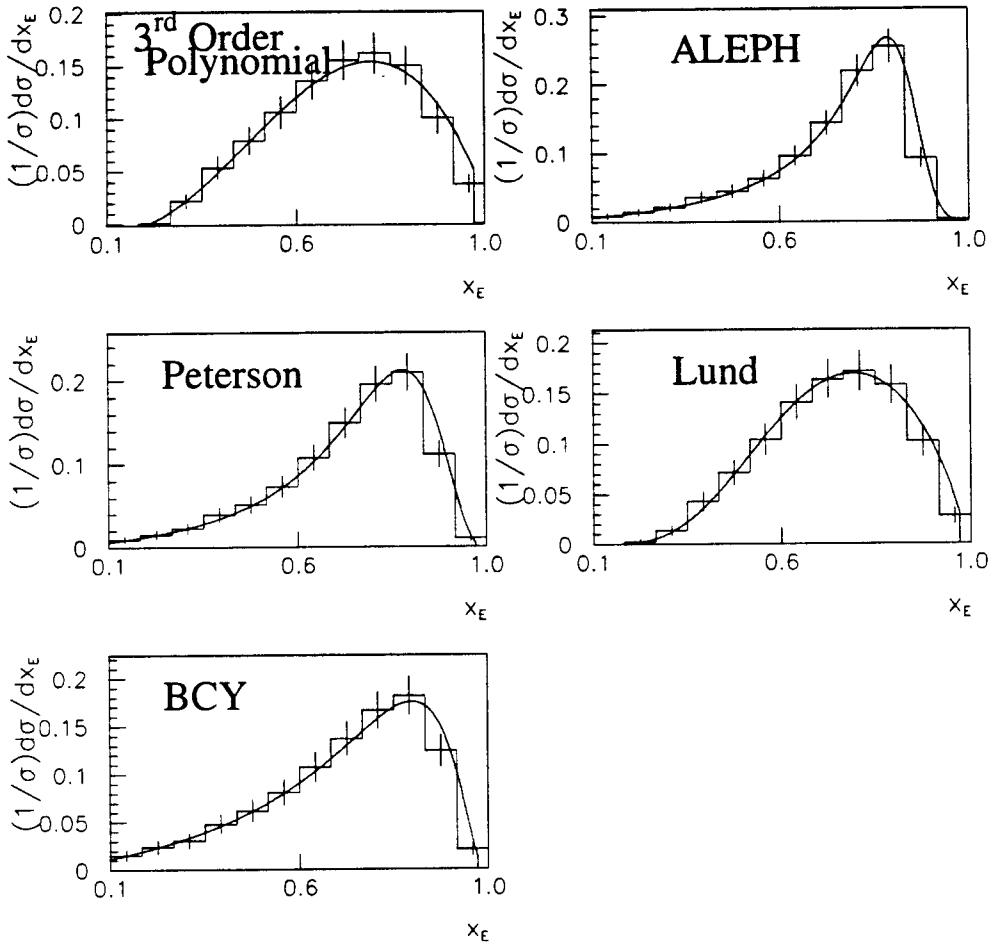

Figure 6: $\mathbf{D}_{\mathbf{True}}^{\mathbf{data}}$, unfolded with the five separate functions. Overlaid are the fits at the final iteration, showing that each gives a good fit. The error bars indicate uncorrelated statistical errors only.

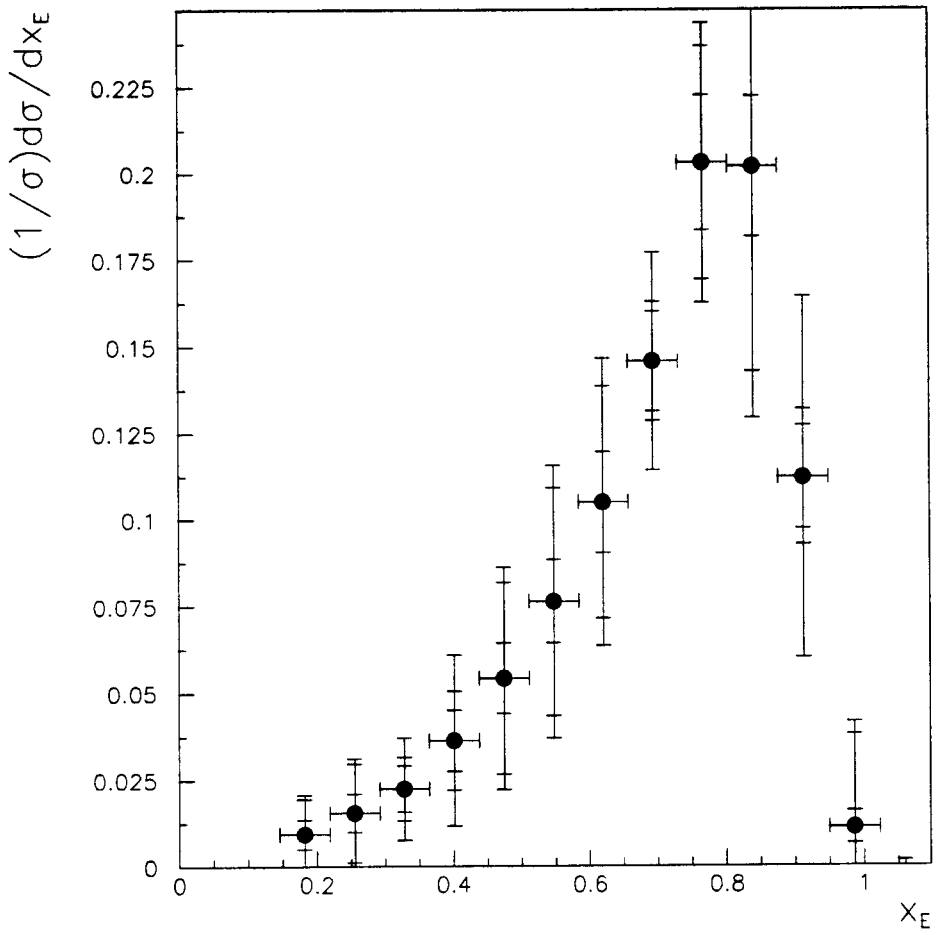

Figure 7: The normalized distribution $\mathbf{D}_{\mathbf{True}}^{\mathbf{data}}$. The inner error bars are statistical errors. The middle ones show the statistical plus function-dependent errors. The outer error bars include all systematic errors.

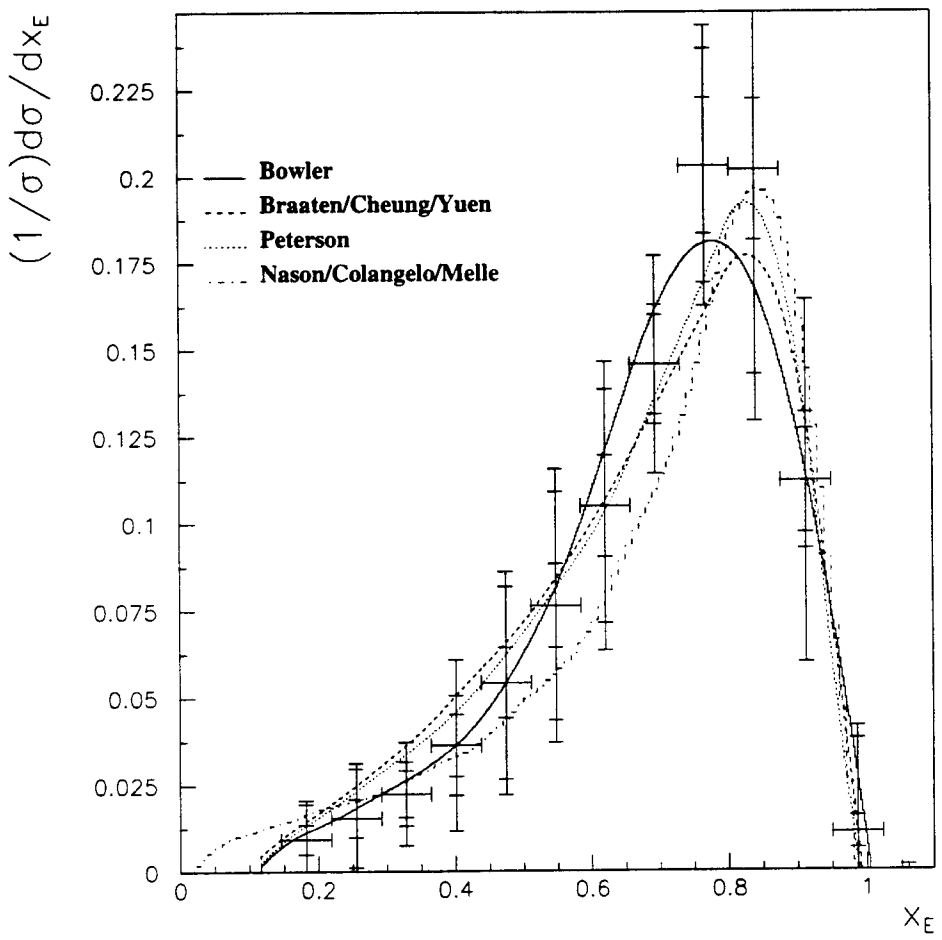

Figure 8: As Figure 7. Overlaid are predictions of four theoretical models. In the first three curves the calculated function in the variable *z* has been transformed into the measurable one in terms of x_E using JETSET7.4. The fourth curve labeled "Nason/Colangelo/Mele" [6] is calculated directly in terms of the measured variable x_E using a program provided by P. Nason.

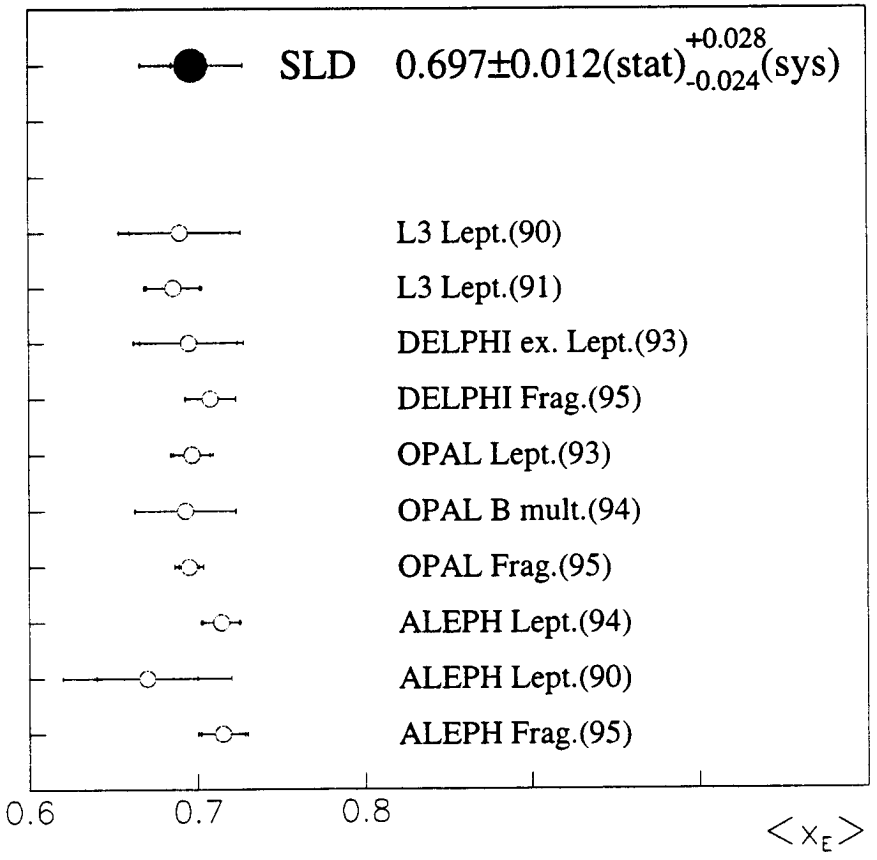

Figure 9: Our measured $\langle x_E \rangle$ together with LEP results [2, 3,4, 33]. Statistical errors are indicated by the inner error bars, and the total error is shown by the outer error bars.